Traffic 2011; **12:** 1407–1416

doi:10.1111/j.1600-0854.2011.01241.x

The Generation of Curved Clathrin Coats from Flat Plaques

Wouter K. den Otter* and Wim J. Briels*

Computational BioPhysics, University of Twente, P.O. Box 217, Enschede 7500 AE, The Netherlands
**Corresponding authors: Wouter K. den Otter, w.k.denotter@utwente.nl and Wim J. Briels, w.j.briels@utwente.nl*

Flat clathrin lattices or 'plaques' are commonly believed to be the precursors to clathrin-coated buds and vesicles. The sequence of steps carrying the flat hexagonal lattice into a highly curved polyhedral cage with exactly 12 pentagons remains elusive, however, and the large numbers of disrupted interclathrin connections in previously proposed conversion pathways make these scenarios rather unlikely. The recent notion that clathrin can make controlled small conformational transitions opens new avenues. Simulations with a self-assembling clathrin model suggest that localized conformational changes in a plaque can create sufficiently strong stresses for a dome-like fragment to break apart. The released fragment, which is strongly curved but still hexagonal, may subsequently grow into a cage by recruiting free triskelia from the cytoplasm, thus building all 12 pentagonal faces without recourse to complex topological changes. The critical assembly concentration in a slightly acidic *in vitro* solution is used to estimate the binding energy of a cage at 25–40 $k_B T$/clathrin.

Key words: clathrin, endocytosis, membrane trafficking, modeling, simulations

Received 20 September 2010, revised and accepted for publication 28 June 2011, uncorrected manuscript published online 1 July 2011, published online 24 July 2011

Clathrin plays important regulatory and structural roles in the formation of cargo-laden vesicles during endocytosis (1–3). Three long curved legs emanating from a hub (Figure 1) enable clathrin to self-assemble into polyhedral cages with a hub residing at every lattice vertex and legs extending along the edges till beyond the next-nearest vertex (4,5). Consequently, every edge consists of a slightly twisted quartet of two antiparallel proximal and two antiparallel distal leg segments (6,7), while the polyhedron's faces are predominantly pentagons and hexagons and occasionally heptagons (8,9). Euler's theorem then dictates that a cage must contain exactly 12 pentagons, with an additional pentagon for every heptagon. The curvature of the cage reflects the puckered shape of clathrin (10), as illustrated in Figure 1. Hence, one readily envisages how a nucleation-and-growth mechanism, by recruiting cytosolic clathrin to the edge of a budding lattice, produces nearly spherical clathrin coats.

Curiously, clathrin also assembles into flat hexagonal lattices, henceforth called 'plaques', as illustrated by cryo electron microscopy (cryo-EM) images (8,11,12). This lattice structure suggests that the three legs are approximately coplanar, in contrast to the puckered shapes of loose clathrin and of clathrin bound in cages (we note that a hexagonal ordering of puckered clathrin will produce a similar top view as a lattice of planar triskelia – the implications of this study on an aggregate of this type are commented on in the *Discussion*). It is commonly believed that plaques are an intermediate stage in the formation of coated vesicles, but the mechanism by which a flat lattice transforms into a polyhedral cage is still under debate as current experimental techniques have insufficient resolution to watch the process in live cells (13). The main conceptual problem is in understanding how the 12 pentagons are introduced into the existing hexagonal lattice. Two pathways have been proposed in which the pentagons are created by the relatively weakly bound clathrin triskelia at the edge of the lattice. Pearse and Bretscher (14) suggested that these pentagons subsequently move inward by diffusion and McKinley (15) argued that the pentagons are embraced by clathrin molecules milling around the edge of the lattice. Other mechanisms assume that pentagons are created in the interior of the lattice by two neighboring hexagons rearranging into a pentagon–heptagon pair. For this scenario, Pearse and Bretscher (14) suggested that the heptagons subsequently diffuse to the lattice edge, while the pentagons stay behind; Mashl and Bruinsma (16) analytically derived that the unbinding of a pentagon–hexagon pair may indeed bring a tethered surface to an energetically more favorable state. The stepwise displacement of a pentagon or heptagon in these hypothesized pathways, and the concomitant modification of the curvature of the lattice, requires a significant number of bonds - not limited to the direct neighbors of the defect - to be broken and next to be reconnected in a slightly modified packing order. Furthermore, this process must be repeated many times to transform a flat lattice into a closed cage, making these pathways extremely unlikely (16,17). These complications are reduced if the insertion of two clathrin molecules in a hexagon can create a pentagon pair, as proposed by Jin and Nossal (18), but this process results in strong local tensions and necessitates puckers well below 90°. Kirchhausen and co-workers recently argued that flat plaques are internalized as such, without reorganization of the lattice (13,19), which raises new questions and 'has given cell biologists much to ponder' (20).

In this contribution, computer simulations are used to explore the transition path from plaque to coat. By making as few assumptions as possible in constructing the

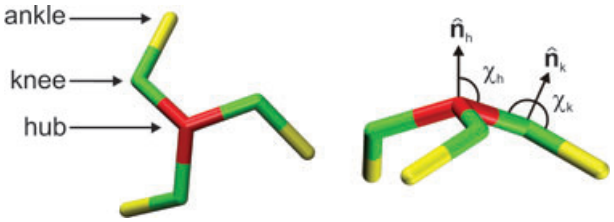

Figure 1: Top and side view illustrating the spatial structure of the clathrin simulation model. All three proximal legs meet at the hub (red) under a pucker angle χ_h relative to the hub's normal vector $\hat{n}_h$. The proximal and distal leg segments joined at a knee (green) are both under a pucker angle χ_k relative to the knee's normal vector $\hat{n}_k$. The latter vector by construction lies in the plane formed by the proximal leg and the hub's normal vector, at an angle χ_k relative to the proximal leg. A rotation around the hub normal over 120° brings a proximal leg in coverage with the next proximal leg. Likewise, a proximal leg can be brought into coverage with the adjacent distal leg by a rotation around a knee normal over 120°. In flat hexagonal lattices or 'plaques' of clathrin, all leg segments are nearly coplanar and hence all pucker angles are close to 90°. Uniformly, puckered triskelia with $\chi_h = \chi_k = 100°$ (or 104°) will self-assemble into polyhedral cages of about 80 (or 36) particles.

model, and by allowing the clathrin cluster to evolve without imposing preconceptions on the transition process, it is to be expected that the simulations will closely follow the actual conversion process. The simulation model is briefly explained in the following section. Our main hypothesis is that a modest flexibility, which for computational convenience is here assumed to be concentrated at the hub and knees, allows clathrin to adopt two 'conformations': a nearly planar conformation found in plaques, with pucker angles $\chi_h = \chi_k = 90°$, and the curved conformation found in cages, with pucker angles ranging from about 100° to 105° depending on the cage size. Numerous studies support the notion that clathrin posseses a modest degree of conformational variability at the hub and knee joints (4–6, 21–26), augmented by semiflexibility along the entire length of the legs (27–29). The simulations of plaques presented in the section *Simulation Results* illustrate that moving from the planar to the curved conformation is all that is needed to yield a stand-alone clathrin dome, adjacent to the remainder of the plaque. In the *Discussion* section, we elaborate on the possible mechanism involved in clathrin's conformational transition, and make comparisons with remarkably similar structures observed by cryo-EM.

Simulation Model

An efficient highly coarse-grained simulation model of clathrin has recently been developed in our group. We discuss here the main features of the model, referring the reader to *Appendix 1: Details of the Simulation Model* and Refs (30,31) for detailed descriptions and a motivation. The simulation model follows clathrin's characteristic shape (Figure 1), with three long legs meeting at a central hub. Note that the term 'hub' is used in this article to denote the central section of the triskelion, roughly coinciding with the red section in Figure 1, rather than the recombinant 1074-1675 fragment used in many experiments. Each leg consists of a proximal leg segment, running from hub to knee, and a distal segment, running from knee to ankle. For computational convenience, all leg segments are assumed straight, rigid, and of identical length σ. All three proximal leg segments are at a fixed pucker angle χ_h relative to the hub's normal vector, which points outward along the threefold rotational symmetry axis of the triskelion. The proximal and distal leg segments meeting at a knee are both at a fixed pucker angle χ_k relative to the knee's normal vector, as indicated in Figure 1. We will typically chose the hub and knee puckers to have identical values, which in our preceding study resulted in the self-assembly of neat polyhedral cages, but we will also briefly discuss triskelia with distinct hub and knee puckers. The puckers are fixed during the Monte–Carlo simulations, reducing the particles to rigid bodies.

The interactions between the legs were constructed in Ref. (30) to achieve self-assembly into clathrin-like cages. Attractive interactions, with an optimum bond strength of $-\varepsilon$, are defined between antiparallel proximal legs and between antiparallel distal legs, to attain the characteristic antiparallel ordering of these segments along the edges of a clathrin cage (5). Details of the applied potential are provided in *Appendix 1: Details of the Simulation Model* and Ref. (30). Attractive interactions are also introduced between proximal and distal pairs, irrespective of their parallel or antiparallel alignment. The smooth shape of the potentials provides some freedom for suboptimal alignment or coalescence of the legs, which is inevitable when constructing a cage from rigid particles, permits the small variations in edge lengths in polyhedrons, and qualitatively accounts for moderate shape fluctuations of the legs. Repulsions between parallel proximal and between parallel distal segments prevent the accumulation of more than four leg segments along any cage edge, and thereby permit at most one clathrin hub per lattice vertex. Monte–Carlo simulations (32,33) with this model have highlighted asymmetric intersegmental interactions, i.e. the nonuniformity of the attractive potential along the elliptic circumference of the legs, as the key to self-assembling cages (30,31). This feature sets clathrin apart from simpler triskelia with uniform, nondirectional interactions, which merely form disordered aggregates.

Simulation Results

As the binding strengths involved in clathrin cage formation have unfortunately not yet been resolved experimentally, we analyzed the assembly and disassembly behavior of the simulation model to estimate the overall interaction strength. The experimental critical assembly concentration (CAC) in a slightly acidic solution of pH

6.2 containing 20 mM $MgCl_2$ is ~50 μg/mL (22). Solutions below the CAC contain predominantly free clathrin and relatively few cages, while for solutions above the CAC the concentration of free clathrin stabilizes at the CAC with all excess clathrin bound in cages. We ran simulations with 10^4 particles at a concentration of 1 particle/$10^3\sigma^3$, which corresponds to about three times the CAC, to analyze the assembly behavior over a range of leg–leg interactions. When the bond strength was increased stepwise, self-assembly from random solution within 10^{11} Monte–Carlo steps was first observed at $\varepsilon = 7¼\ k_BT$, with k_B the Boltzmann constant and T the absolute temperature. Upon weakening the interactions, a collection of self-assembled cages started to disintegrate at $\varepsilon = 5.0\ k_BT$. The difference between these assembly and disassembly energies reflects the inevitable hysteresis effect in simulations limited by computational demands. By averaging the two bracketing values, we estimate that the critical bond strength for assembly at a density of 1 particle/$10^3\sigma^3$ is about 6 k_BT. In simulations of random systems seeded with 12 hemispherical cages, the majority of these aggregation nuclei slowly grew (decayed) at binding strengths of ¼ k_BT above (below) the critical value of 6 k_BT, thereby confirming the estimate. Hence, by switching from variable interaction strength at constant density to variable density at constant interaction strength, particles with $\varepsilon = 6\ k_BT$ will reach criticality at a concentration close to clathrin's experimental CAC of 50 μg/mL. Because the relative contributions of the proximal and distal segments are unknown, and as it is impossible for all legs of identical rigid triskelia to be perfectly aligned in a polyhedral cage, the relevant parameter to compare with experiments is not the maximum interaction energy ε but the average interaction energy per clathrin. At $\varepsilon = 6\ k_BT$, the potential energy of self-assembled cages corresponds to an average of ~23 k_BT per triskelion. This estimate for the binding strength in slightly acidic solutions is in qualitative agreement with the value of ~42 k_BT obtained by the CAC-based statistical mechanical derivation presented in *Appendix 2: Critical Assembly Concentration*, and both are two orders of magnitude larger than the binding strengths previously extracted from the size distribution of bulk self-assembled cages (34). In most of the simulations presented here, the binding strength was set at a slightly higher value of $\varepsilon = 7\ k_BT$, both to prevent the flat plaques from slow disintegration in an environment without free clathrin and in anticipation of the higher effective binding strengths expected for clathrin lattices stabilized by adaptor proteins in living cells.

In order to simulate planar clathrin plaques, we flattened the model triskelia by reducing their hub and knee puckers to 90°. Monte–Carlo simulations show that random distributions of these planar triskelia readily self-assemble into flat hexagonal lattices (Figure 2) under conditions similar to those reported above for the self-assembly of puckered triskelia into cages. We note that asymmetric intersegmental interactions again prove crucial to the growth process, because replacing the asymmetric potential by its symmetric counterpart results in hexagonal grids littered with defects such as the first planar aggregate shown in Figure 2.

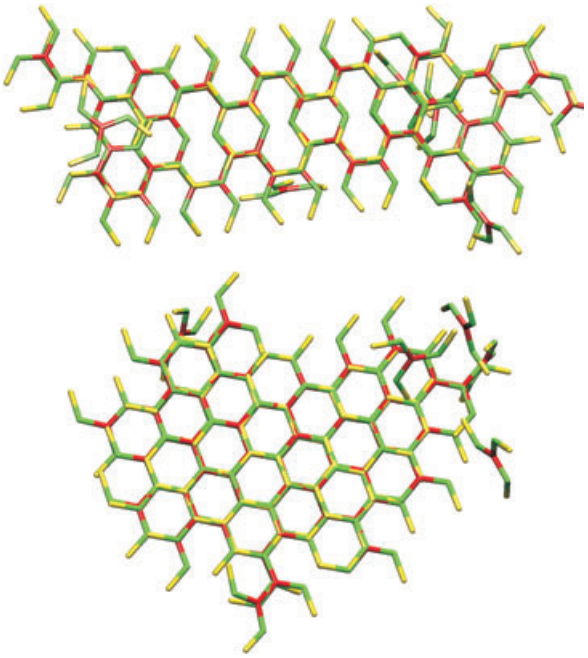

Figure 2: Snapshots of self-assembled planar lattices in simulations with flat clathrin. Triskelia with rotationally symmetric intersegmental interactions (top) yield lattices with many defects because the clathrin molecules are incorporated in two orientations, i.e. with their normals pointing in-to or out-of the paper, which appear as mirror images in the picture. Clathrin with rotationally asymmetric intersegmental interactions (bottom) produce well-structured hexagonal lattices with all clathrins oriented identically.

In the introduction, we hypothesized that clathrin can adopt two conformations, a planar conformation found in plaques and a curved conformation found in cages. We will now use the simulation model to explore the consequences of this conformational freedom on the transition pathway from plaque to coat. Figure 3 shows an equilibrated circular lattice of about 10 σ radius, containing 243 planar triskelia positioned as a hexagonal lattice with a mean mesh size equal to the length of the leg segments. The hub and knee puckers of the 59 triskelia in the red patch on the right, all falling within a circle of radius 8 σ around the rightmost point of the lattice, are instantaneously increased from 90° to 100° to emulate their conformational transitions to the curved coat conformation. In making these transitions, we preserved the center of mass positions, the hub normal orientations and the rotations of the particles around the hub normals. As the curved clathrin triskelia prefer a uniformly curved lattice because of its lower potential energy, that is what the system sets forth to realize in the Monte–Carlo simulation started with this configuration. As illustrated in Movie S1, covering 1.5×10^7 Monte-Carlo steps, the red patch

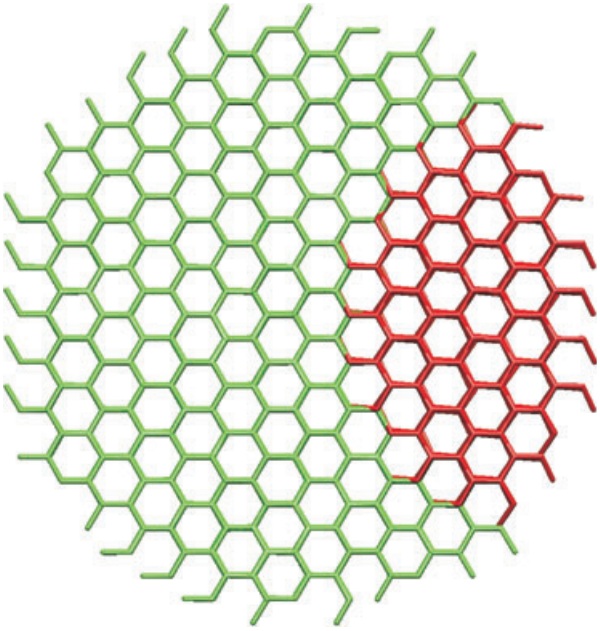

Figure 3: A planar hexagonal clathrin plaque of ∼10 σ radius. The green clathrin molecules on the left are flat, with all puckers set to $\chi_h = \chi_k = 90^\circ$, as expected for a flat plaque. The puckers of the red clathrin molecules on the right have instantaneously been increased from 90° to $\chi_h = \chi_k = 100^\circ$, in line with the hypothesized transition from a plaque-like to a coat-like conformation, while preserving as much as possible their position and orientation within the originally fully hexagonal lattice.

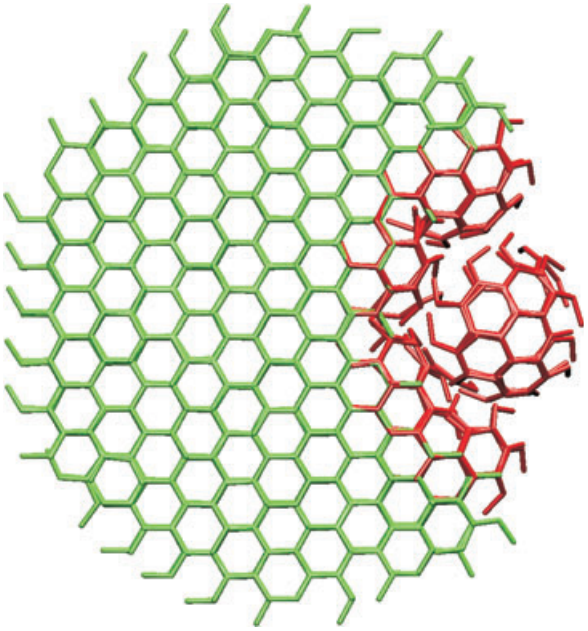

Figure 4: The planar plaque of Figure 3 succumbs to internal stresses and a dome-like fragment breaks away. The deformation and rupture process, due to the incompatibility of flat (green) and curved (red) triskelia, is available in Movie S1. The released dome, containing only hexagonal faces, can subsequently grow into a full cage by binding additional cytosolic clathrin at its rim. The 12 pentagonal faces of a completed cage are incorporated in this later stage.

of puckered triskelia gradually warps and bends, and thus induces significant transverse stresses in the mesh. The gradually increasing curvature distorts and thereby weakens the bonds between the curved patch and the flat plaque. The combination of constant segmental lengths with an increasing curvature causes the patch to contract laterally, which adds to the tensions in the lattice. Once the collective build-up of tensions exceeds a critical value, a curved patch can break apart from the remaining lattice. The fragment continues to curve after its release, culminating in the situation depicted in Figure 4: a dome at the center of a semicircular frayed lattice edge. The separated fragment initially still contains merely hexagonal faces, but the high curvature of the patch now makes it possible for the dangling legs at the edges, brought together by the lattice curvature, to meet and occasionally bind to form pentagons. Similar highly curved domains, frequently followed by the liberation of a dome-like fragment, were observed across a series of simulations with various pucker angles, for different sizes of the activated and planar domains, and under varying bond strengths. The rupture line separating the dome from the mother plaque invariably lies within the lattice segment of curved triskelia, and hence a newly release fragment contains puckered triskelia only.

Further maturation of the newly created dome into a fully grown coat will most probably be achieved by binding additional free triskelia from the cytoplasmic pool, like for cages developed by the usual nucleation-and-growth scenario, and perhaps supplemented by clathrin released from the edge of the remaining plaque. The 12 pentagons required to close the polyhedral cage will mainly be created during this growth phase, and without resorting to complex lattice reshuffling. On the basis of the average cage size for self-assembling cages (31) of $\chi = 100^\circ$ triskelia, the released fragment of about 20 particles is expected to acquire an additional ∼60 clathrin molecules before cage completion, which should offer many possibilities to incorporate the additional pentagons required for closure. Note that in this scenario the pentagons will be unevenly distributed over the surface of the polyhedron: they are scarce in the cage section originating as the released plaque fragment, while pentagons are overrepresented in the remainder of the cage. Hence, these cages are probably less spherically symmetric than cages assembled by the regular nucleation-and-growth process, and one may readily envisage a situation where the incoming clathrin adapts a different curvature than the clathrin in the dome to produce a lopsided coat. In the extreme case of all attaching triskelia adopting a nearly flat conformation, the fragment will grow into a conical or cylindrical structure. We expect that the growing fragment and the mother plaque are not likely to fuse again, because the difference in their curvatures prevents strong binding.

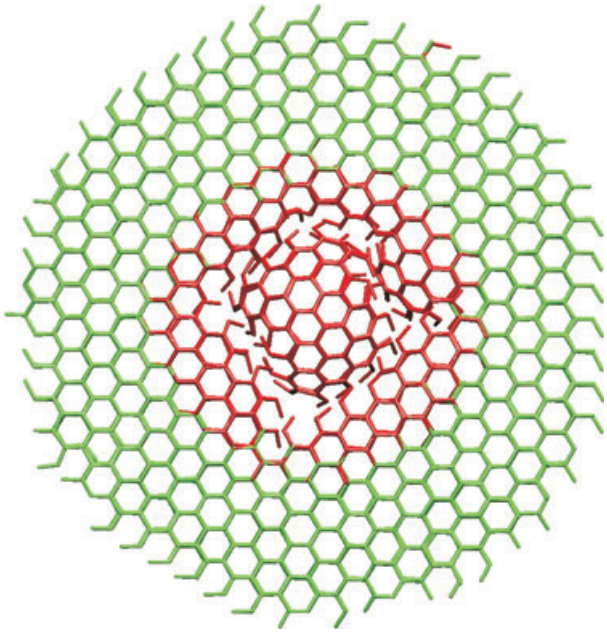

Figure 5: A dome released from the interior of a plaque. This scenario occurs if the patch of curved clathrin triskelia (red) happens to be located in the bulk rather than at the edge of the lattice. Note that the edge must be strong enough, i.e. the ring of flat clathrin molecules (green) must be sufficiently wide, to prevent the ring from yielding under the tension. The single red clathrin near the top detached from a frayed edge and wandered around for some time before reconnecting to the edge of the plaque.

We also explored how a plaque evolves when the patch of nonflat clathrin is located in the middle rather than at the edge of an equilibrated flat lattice. A patch of curved triskelia initially surrounded by flat lattice along its entire circumference is stronger bounded to the planar remainder of the plaque than a similar-sized patch at the edge of a plaque. Simulations of a number of these systems indicate, nevertheless, that a central patch of curved triskelia can still follow a similar scenario to the one outlined in the previous section, and thereby produce a detached dome in the interior of the plaque, as illustrated in Figure 5. Again, the newly produced cage fragments may subsequently grow into full cages by binding free clathrin from the cytosol and additional triskelia released from the plaque.

By changing the curvature of a fraction of randomly selected clathrin across a flat lattice, or by varying the curvature of all triskelia in a plaque, one obtains a wide assortment of lightly to strongly contorted lattices, as illustrated in Figure 6. The simulations indicate that a hexagonal lattice can withstand a surprisingly high curvature before disentangling, in agreement with experimental observations (8). Interestingly, in some cases the lattice does not bend uniformly in both directions, but instead yields in one random direction only and adopts a semi-cylindrical shape; presumably this shape strengthens the

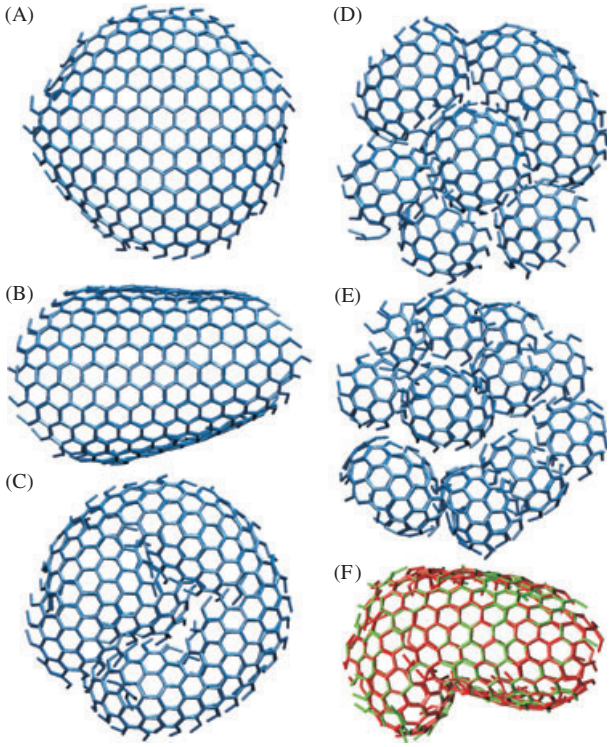

Figure 6: A single plaque can become contorted and fragmented in a variety of ways. Each simulation started with the same circular hexagonal lattice of 253 triskelia and ~10 σ radius. The hub and knee puckers of the triskelia are (A) 95°, (B) 95°, (C) 97°, (D) 98° and (E) 99°, and (F) a random mixture of 70% particles with puckers of 100° (red) and 30% particles with puckers of 90° (green). Note the resemblance to Heuser's cryo-EM images of clathrin lattices on membrane fragments in neutral and acidic media (11).

structure against bending in the perpendicular direction. Large lattices of curved clathrin break up into several fragments (Figure 6), as this is the only way to resolve the conflicting interests between neighboring curved sections within these patches. The simulations indicate that the number of fragments increases, and their size diminishes, with increasing curvature of the nonplanar triskelia, with increasing ratios of curved to non-curved clathrin and with increasing patch size. Fragmentation into multiple domes was also observed for patches of curved triskelia initially bound to a planar lattice.

Simulations of random solutions of nonuniformly curved triskelia, i.e. particles with their hub puckers differing from their knee puckers, reveal that these self-assemble into polyhedral cages just as readily as the above discussed uniformly curved triskelia, i.e. with equal hub and knee puckers. In the latter case, the preferred average cage size is clearly determined by the singular pucker value, and a relation between the two has been derived in Ref. (31). For nonuniformly puckered clathrin with hub puckers fixed at 105°, it still proved feasible to grow cages of various small and medium sizes by varying the

knee pucker only, in line with the observation by Fotin et al. (5) that the hub pucker is invariant across 16 distinct vertices in several small cages. For completeness, we note that the sizes of coats grown in endocytosis are determined by the dimensions of the enveloped cargo, within limits set by clathrin flexibility, rather than by the fixed triskelion geometry employed in the current simulations. Having established their ability to self-assemble into cages, we next turn to plaques containing nonuniformly particles.

We studied the progress of patches of curved clathrin initially attached to a flat lattice, akin to the system in Figure 3, when the hub and knee puckers are changed independently of one another. The general trend extracted from an extensive set of simulations is that increasing the hub pucker at a fixed knee pucker of 90°, or increasing the knee pucker at a constant hub pucker of 90°, introduces a significant curvature in the lattice. Whether or not the imparted curvature is strong enough to release a fragment from the flat lattice depends in an intricate way on a large number of parameters including the values of the altered pucker, the size and shape of the affected patch, the size and shape of the planar section of the lattice and the leg–leg interaction strength ε. The general impression after running and visualizing many simulations is that patches of uniformly curved triskelia undergoing a pucker change $\Delta\chi_u$ and patches of nonuniformly curved particles experiencing a pucker change $\Delta\chi_{nu}$ at either joint release dome-like fragments under comparable conditions, provided $\Delta\chi_{nu} = 2\Delta\chi_u$. This suggests that the overall curvature of the triskelion, rather than the pucker of specific joint, is an important parameter determining the fate of the system.

Discussion

The notion that the hub and knee joints of clathrin provide the modest flexibility required to build cages of various shapes and sizes is well established. Small cages, like the cubes (26) and tetrahedrons (21) grown *in vitro*, clearly highlight clathrin's flexibility at both the hub and knee. Cryo-EM anaglyph stereo images by the groups of Heuser and Ungewickell show remarkably flat hexagonal lattices, suggesting that clathrin is sufficiently flexible to adopt a near-planar conformation. The simulations presented here indicate that, if clathrin molecules can also change their curvature *in vivo*, a flat plaque is much more likely, from a statistical physical point of view, to follow a pathway in which it releases a curved fragment rather than a scenario in which a complete plaque evolves into a single cage by repeatedly and thoroughly reshuffling its clathrin triskelia. The pathway found by the simulations implies that the pentagonal faces, which are rare in plaques but crucial to the formation of closed cages, are produced after the release of a dome-like segment by free cytosolic triskelia binding to the edge of the partial cage, thereby altogether avoiding the topological constraints that make the hypothesized introduction of pentagons by lattice reshuffles an unlikely process.

Further research may establish whether and how the clathrin molecules in a plaque, confined as they are to the interior of the cell, perceive the presence of cargo and alter their conformation. Recent experiments by Brodsky et al. (25) and Ybe et al. (24) and Ybe (private communication) indicate that clathrin light chains might be involved in regulating the conformations of the knee and hub, respectively, and thus are possibly implicated in the initiation of the conformational changes at the basis of our working hypothesis. These conformational switching mechanisms appear to support the observations that clathrin is essential for driving coated pit invagination (35). In this context, we note that the clathrin coat, with four α-solenoidal legs running along every cage edge, has a much more sturdily built than the COPII coat with a single α-solenoidal leg per edge (36,37).

At this point, we cannot conclusively rule out that plaques *in vivo* may be membrane-bound assemblies of puckered clathrin molecules, in contrast to the clearly planar lattices observed on membranes supported by flat substrates. An array of puckered triskelia can still appear as a hexagonal lattice in the top view, while the side view will show a forest of crisscrossing legs. This assembly might be stable if, for instance, steric constraints between the legs prevent the necessarily poorly aligned legs from forming stronger bonds. Lifting these constraints, which may be brought about by a conformational change of the knees through the detachment of a light chain (25), will then result in a potential energy-driven improved alignment of legs belonging to neighboring puckered clathrin triskelia and thereby initiate a curve-and-release pathway similar to that described in the previous section.

Besides changes in the puckers of the hub and knees, the flexibility of the leg segments (27–29) may contribute to or give rise to the hypothesized conformational transitions. The flexibility of the legs is expected to be beneficial in the restructuring process, by smoothing the breaking and reformation of leg–leg connections. It is conceivable that membrane-bending proteins, such as epsins or BAR domains (38,39), play a supporting or important role by bending the membrane and thereby promote curvature of the clathrin lattice. The release of clathrin molecules from a lattice or partial cage by uncoating proteins (40-44) may play a facilitating role in remodeling the dome's edge. It is unlikely, however, that spontaneous exchange of triskelia is capable of changing hexagons into pentagons in the interior of a lattice, as has been suggested in Ref. (18). This is because topological restraints demand that a significant number of adjacent triskelia have to be replaced concurrently to locally alter the lattice structure for this mechanism to work, which is energetically not attractive. Instead, our simulations suggest that domes in the middle of a lattice, as well as those at the edge, are

created by strain causing a fragment to break loose from the flat lattice, allowing new triskelia to join the assembly.

Dome-like clathrin structures adjacent to plaques, which following the mechanism observed in the simulations will emerge at an intermediate stage in the sprouting of coated vesicles from plaques, have been observed by cryo-EM. These domes are typically located at the edge of a plaque, where the lattice is at its weakest and where diffusing membrane-bound cargo is most likely to first come into contact with the endocytic machinery (11,45,46). Two particularly clear cryo-EM images of domes bordering flat plaques, copied from Refs (21) and (44), are presented in Figure 7. In both cases, the plaque has a frayed semicircular edge curving around a dome, strongly suggesting that the dome used to be an integral part of the plaque before it was torn away and curled up. The strong resemblance between these experimental structures and our simulated structures (Figure 4) indicates that we are most likely dealing with the same mechanism in both cases. Likewise, the contorted and fragmented lattices in Figure 6 are reminiscent of Heuser's cryo-EM pictures (11) of plaques on membranes in neutral and acidic media. It is a challenge to clathrin researchers to explore whether further experimental evidence in favor of, or against, this novel pathway can be found.

Finally, we note that the curve-and-release scenario explains how a flat plaque bound to a membrane can act as a 'hot spot' sprouting multiple clathrin coats, for as long as clathrin recruitment by the plaque can compensate for the losses in released domes (47-49).

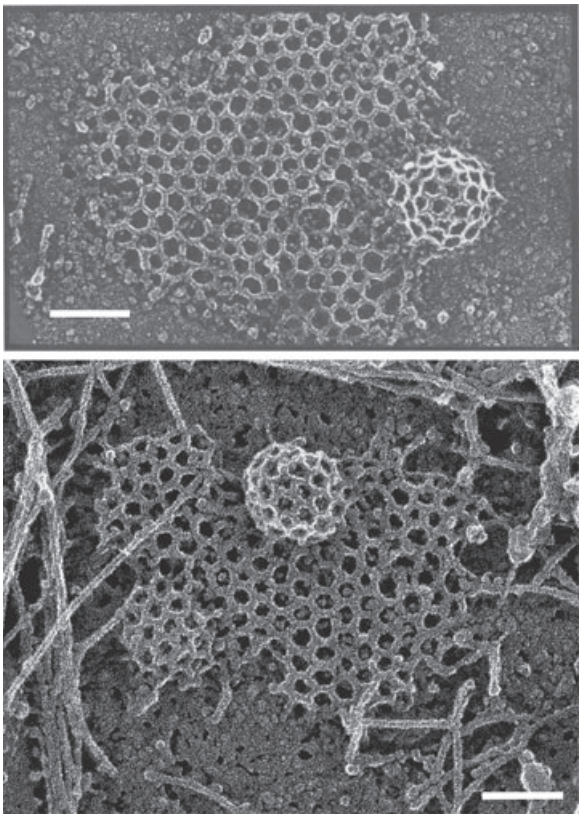

Figure 7: Cryo-EM images of coated pits that appear to have broken away from flat plaques. The hemispherical domes are positioned at the centers of semicircular frayed lattice edges, in striking resemblance to Figure 4. Bars: 100 nm. Figures are reproduced from Ref. (21; top) and Ref. (44; bottom) with permission.

Supporting Information

Additional Supporting Information may be found in the online version of this article:

Movie S1: The movie shows how the initially flat hexagonal lattice of Figure 3, with the planar clathrins ($\chi_h = \chi_k = 90^\circ$) colored green and the puckered clathrins ($\chi_h = \chi_k = 100^\circ$) in red, develops into the state depicted in Figure 4 by releasing a dome-like fragment.

Please note: Wiley-Blackwell are not responsible for the content or functionality of any supporting materials supplied by the authors. Any queries (other than missing material) should be directed to the corresponding author for the article.

References

1. Royle SJ. The cellular functions of clathrin. Cell Mol Life Sci 2006; 63:1823–1832.
2. Schmid EM, McMahon HT. Integrating molecular and network biology to decode endocytosis. Nature 2007;448:883–888.
3. Edeling MA, Smith C, Owen D. Life of a clathrin coat: insights from clathrin and AP structures. Nat Rev Mol Cell Biol 2006;7:32–44.
4. Ungewickell E, Branton D. Assembly units of clathrin coats. Nature 1981;289:420–422.
5. Fotin A, Cheng YF, Sliz P, Grigorieff N, Harrison SC, Kirchhausen T, Walz T. Molecular model for a complete clathrin lattice from electron cryomicroscopy. Nature 2004;432:573–579.
6. Musacchio A, Smith CJ, Roseman AM, Harrison SC, Kirchhausen T, Pearse BMF. Functional organization of clathrin in coats: combining electron cryomicroscopy and x-ray crystallography. Mol Cell 1999;3:761–770.
7. Wilbur JD, Hwang PK, Brodsky FM. New faces of the familiar clathrin lattice. Traffic 2005;6:346–350.
8. Heuser J. Three-dimensional visualization of coated vesicle formation in fibroblasts. J Cell Biol 1980;84:560–583.
9. Kanaseki T, Kadota K. The ''vesicle in a basket'' - a morphological study of the coated vesicle isolated from nerve endings of the guinea pig brain, with special reference to the mechanism of membrane movements. J Cell Biol 1969;42:202–220.
10. Kirchhausen T, Harrison SC, Heuser J. Configuration of clathrin trimers - evidence from electron-microscopy. J Ultrastruct Mol Struct Res 1986;94:199–208.
11. Heuser J. Effects of cytoplasmic acidification on clathrin lattice morphology. J Cell Biol 1989;108:401–411.
12. Maupin P, Pollard TD. Improved preservation and staining of Hela-cell actin-filaments, clathrin-coated membranes, and other cytoplasmic structures by tannic-acid glutaraldehyde-saponin fixation. J Cell Biol 1983;96:51–62.
13. Kirchhausen T. Imaging endocytic clathrin structures in living cells. Trends Cell Biol 2009;19:596–605.
14. Pearse BMF, Bretscher MS. Membrane recycling by coated vesicles. Annu Rev Biochem 1981;50:85–101.
15. McKinley DN. Model for transformations of the clathrin lattice in the coated vesicle pathway. J Theor Biol 1983;103:405–419.
16. Mashl RJ, Bruinsma RF. Spontaneous-curvature theory of clathrin-coated membranes. Biophys J 1998;74:2862–2875.

17. Kirchhausen T. Coated pits and coated vesicles - sorting it all out. Curr Opin Struct Biol 1993;3:182–188.
18. Jin AJ, Nossal R. Topological mechanisms involved in the formation of clathrin-coated vesicles. Biophys J 1993;65:1523–1537.
19. Saffarian S, Cocucci E, Kirchhausen T. Distinct dynamics of endocytic clathrin-coated pits and coated plaques. PLoS Biol 2009;7:e1000191.
20. Traub LM. Clathrin couture: fashioning distinctive membrane coats at the cell surface. PLoS Biol 2009;7:e1000192.
21. Heuser JE, Keen JH, Amende LM, Lippoldt RE, Prasad K. Deep-etch visualization of 27S-clathrin - a tetrahedral tetramer. J Cell Biol 1987;105:1999–2009.
22. Crowther RA, Pearse BMF. Assembly and packing of clathrin into coats. J Cell Biol 1981;91:790–797.
23. Yoshimura T, Kameyama K, Maezawa S, Takagi T. Skeletal structure of clathrin triskelion in solution - experimental and theoretical approaches. Biochemistry 1991;30:4528–4534.
24. Ybe JA, Perez-Miller S, Niu Q, Coates DA, Drazer MW, Clegg ME. Light chain C-terminal region reinforces the stability of clathrin heavy chain trimers. Traffic 2007;8:1101–1110.
25. Wilbur JD, Hwang PK, Ybe JA, Lane M, Sellers BD, Jacobson MP, Fletterick RJ, Brodsky FM. Conformation switching of clathrin light chain regulates clathrin lattice assembly. Dev Cell 2010;18:841–848.
26. Sorger PK, Crowther RA, Finch JT, Pearse BMF. Clathrin Cubes - an extreme variant of the normal cage. J Cell Biol 1986;103:1213–1219.
27. Ferguson ML, Prasad K, Boukari H, Sackett DL, Krueger S, Lafer EM, Nossal R. Clathrin triskelia show evidence of molecular flexibility. Biophys J 2008;95:1945–1955.
28. Kotova S, Prasad K, Smith PD, Lafer EM, Nossal R, Jin AJ. AFM visualization of clathrin triskelia under fluid and in air. FEBS Lett 2010;584:44–48.
29. Jin AJ, Nossal R. Rigidity of triskelion arms and clathrin nets. Biophys J 2000;78:1183–1194.
30. den Otter WK, Renes MR, Briels WJ. Asymmetry as the key to clathrin cage assembly. Biophys J 2010;99:1231–1238.
31. den Otter WK, Renes MR, Briels WJ. Self-assembly of three-legged patchy particles into polyhedral cages. J Phys Condens Matter 2010;22:104103.
32. Allen M, Tildesley DJ. Computer Simulation of Liquids. Oxford: Oxford Science Publishers; 1993.
33. Frenkel D, Smit B. Understanding Molecular Simulation. From Algorithms to Applications. San Diego, CA: Academic Press; 2002.
34. Nossal R. Energetics of clathrin basket assembly. Traffic 2001;2: 138–147.
35. Hinrichsen L, Meyerholz A, Groos S, Ungewickell EJ. Bending a membrane: how clathrin affects budding. Proc Natl Acad Sci U S A 2006;103:8715–8720.
36. Stagg SM, LaPointe P, Razvi A, Gurkan C, Potter CS, Carragher B, Balch WE. Structural basis for cargo regulation of COPII coat assembly. Cell 2008;134:474–484.
37. Fath S, Mancias JD, Bi XP, Goldberg J. Structure and organization of coat proteins in the COPII cage. Cell 2007;129:1325–1336.
38. Ford MGJ, Mills IG, Peter BJ, Vallis Y, Praefcke GJK, Evans PR, McMahon HT. Curvature of clathrin-coated pits driven by epsin. Nature 2002;419:361–366.
39. Henne WM, Boucrot E, Meinecke M, Evergren E, Vallis Y, Mittal R, McMahon HT. FCHo proteins are nucleators of clathrin-mediated endocytosis. Science 2010;328:1281–1284.
40. Wu XF, Zhao XH, Baylor L, Kaushal S, Eisenberg E, Greene LE. Clathrin exchange during clathrin-mediated endocytosis. J Cell Biol 2001;155:291–300.
41. Wu XF, Zhao XH, Puertollano R, Bonifacino JS, Eisenberg E, Greene LE. Adaptor and clathrin exchange at the plasma membrane and trans-Golgi network. Mol Biol Cell 2003;14:516–528.
42. Loerke D, Wienisch M, Kochubey O, Klingauf J. Differential control of clathrin subunit dynamics measured with EW-FRAP microscopy. Traffic 2005;6:918–929.
43. Xing Y, Bocking T, Wolf M, Grigorieff N, Kirchhausen T, Harrison SC. Structure of clathrin coat with bound Hsc70 and auxilin: mechanism of Hsc70-facilitated disassembly. EMBO J 2010;29:655–665.
44. Hoffmann A, Dannhauser PN, Groos S, Hinrichsen L, Curth U, Ungewickell EJ. A comparison of GFP-tagged clathrin light chains with fluorochromated light chains in vivo and in vitro. Traffic 2010;11:1129–1140.
45. Larkin JM, Donzell WC, Anderson RGW. Potassium-dependent assembly of coated pits - new coated pits form as planar clathrin lattices. J Cell Biol 1986;103:2619–2627.
46. Signoret N, Hewlett L, Wavre S, Pelchen-Matthews A, Oppermann M, Marsh M. Agonist-induced endocytosis of CC chemokine receptor 5 is clathrin dependent. Mol Biol Cell 2005;16:902–917.
47. Gaidarov I, Santini F, Warren RA, Keen JH. Spatial control of coated-pit dynamics in living cells. Nat Cell Biol 1999;1:1–7.
48. Merrifield CJ, Perrais D, Zenisek D. Coupling between clathrin-coated-pit invagination, cortactin recruitment, and membrane scission observed in live cells. Cell 2005;121:593–606.
49. Bellve KD, Leonard D, Standley C, Lifshitz LM, Tuft RA, Hayakawa A, Corvera S, Fogarty KE. Plasma membrane domains specialized for clathrin-mediated endocytosis in primary cells. J Biol Chem 2006;281:16139–16146.
50. Gelbart WM, Ben-Shaul A, Roux D. Micelles, Membranes, Microemulsions, and Monolayers. New York: Springer Verlag; 1994.
51. Zandi R, van der Schoot P, Reguera D, Kegel W, Reiss H. Classical nucleation theory of virus capsids. Biophys J 2006;90:1939–1948.
52. Zlotnick A. To build a virus capsid - an equilibrium-model of the self-assembly of polyhedral protein complexes. J Mol Biol 1994;241:59–67.
53. Schein S, Sands-Kidner M. A geometric principle may guide self-assembly of fullerene cages from clathrin triskelia and from carbon atoms. Biophys J 2008;94:958–976.

Appendix 1: Details of the Simulation Model

In this appendix we summarize the interactions of the clathrin simulation model, as introduced in Ref. (30). A repeating motif in clathrin cages is the binding of the proximal segment of the α^{th} leg of triskelion i with the antiparallel proximal segment of the β^{th} leg of triskelion j, bringing the hub (h) of leg ($i\alpha$) in close proximity to the knee (k) of leg ($j\beta$) and simultaneously bringing the knee of leg ($i\alpha$) in close proximity to the hub of leg ($j\beta$). It is therefore appealing to introduce the attractive potential between two proximal segments as a function of the average of these two distances,

$$r_{j\beta,\mathrm{kh}}^{i\alpha,\mathrm{hk}} = \frac{1}{2}\left|\mathbf{x}_{i\alpha,\mathrm{h}} - \mathbf{x}_{j\beta,\mathrm{k}}\right| + \frac{1}{2}\left|\mathbf{x}_{i\alpha,\mathrm{k}} - \mathbf{x}_{j\beta,\mathrm{h}}\right|, \qquad (1)$$

with $\mathbf{x}_{i\alpha,\mathrm{k}}$ denoting the three-dimensional position of the knee to the α^{th} leg of particle i and so on. The indices to r mark the two leg segments involved and their relative orientation (antiparallel in this case). In two previous studies, we showed that directional attractive potentials hold the key to successful self-assembly: the two antiparallel legs should bind only when their proper sides, i.e. the surfaces decorated with binding groups, are facing each other (30,31). Hence, a 'polarity' vector perpendicular to the proximal leg indicates its direction of interaction

$$\hat{\mathbf{m}}_{i\alpha,\mathrm{p}} = \frac{(\mathbf{x}_{i\alpha,\mathrm{k}} - \mathbf{x}_{i\alpha,\mathrm{h}}) \times \hat{\mathbf{n}}_{i\alpha,\mathrm{h}}}{|(\mathbf{x}_{i\alpha,\mathrm{k}} - \mathbf{x}_{i\alpha,\mathrm{h}}) \times \hat{\mathbf{n}}_{i\alpha,\mathrm{h}}|}, \qquad (2)$$

with $\hat{\mathbf{n}}_{i\alpha,\mathrm{h}}$ as the previously introduced normal vector at the hub. Note that this polarity is fixed relative to the rigid triskelion and corotates with the particle. The attractive interaction between two antiparallel proximal legs is then expressed as:

$$\phi_{\mathrm{pp}}^{\mathrm{att}} = -\varepsilon \cdot f(r_{j\beta,\mathrm{kh}}^{i\alpha,\mathrm{hk}}) \cdot g(\hat{\mathbf{m}}_{i\alpha,\mathrm{p}} \cdot \hat{\mathbf{m}}_{j\beta,\mathrm{p}}). \qquad (3)$$

The distance-dependent function f smoothly switches from unity at vanishing separation to zero at the cut-off distance r_c,

$$f(r) = \frac{\tanh\left[A\,(r_c/2 - r)\right]}{2\tanh\left[Ar_c/2\right]} + \frac{1}{2}. \tag{4}$$

In the simulations presented here, the interaction range ends at $r_c = 0.4\sigma$ and the steepness of the switch is set at $A = 4\sigma^{-1}$. The polarity-dependent function is defined as:

$$g(x) = \begin{cases} -x & \text{if} \quad x < 0 \\ 0 & \text{if} \quad x > 0. \end{cases} \tag{5}$$

A similar attractive interaction applies between two antiparallel distal leg segments, with the mean distance $r^{i\alpha,\mathrm{ka}}_{j\beta,\mathrm{ak}}$ now measured between the appropriate knees and ankles (a), and the polarities of the distal segments $\hat{\mathbf{m}}_{i\alpha,\mathrm{d}}$ defined akin to eqn 2 as the normalized cross product of the knee–ankle vector of leg ($i\alpha$) and the normal vector of the knee to that leg. Attractive interactions between one proximal and one distal leg segment are defined likewise, although without the polarity dependence. Simulations in which the relative strengths of the various intersegmental interactions were varied indicate that their precise distribution is of little consequence to the ability to self-assemble, provided the total potential energy gained upon clustering is large enough to overcome the concomitant loss of translational entropy (*Appendix 2: Critical Assembly Concentration)*. For the numerical values for ε reported here and in Ref. (30), the unlike interactions are set to half the strength ε of the like interactions.

To prevent a proximal leg from binding with multiple antiparallel proximal legs, we introduce a repulsion between two parallel proximal legs. This potential has the form

$$\phi^{\mathrm{rep}}_{\mathrm{pp}} = -\bar{\varepsilon}\cdot\bar{f}(r^{i\alpha,\mathrm{hk}}_{j\beta,\mathrm{hk}}), \tag{6}$$

where $r^{i\alpha,\mathrm{hk}}_{j\beta,\mathrm{hk}}$ is the average of the two hub–knee distances, and

$$\bar{f}(r) = \frac{\tanh\left[\bar{A}\,(\bar{r}_c/2 - r)\right]}{2\tanh\left[\bar{A}\bar{r}_c/2\right]} + \frac{1}{2}. \tag{7}$$

Note that this repulsion is applied independently of the relative orientation of the legs' polarities. The interaction parameters are set to $\bar{\varepsilon} = -10\varepsilon$, $\bar{A} = \frac{A}{5}$ and $\bar{r}_c = 2r_c$ to make the repulsion strong enough to fulfill its objectives. To prevent distal legs from binding with multiple antiparallel distal legs, we introduce a similar repulsion between pairs of parallel distal legs.

Appendix 2: Critical Assembly Concentration

Solvated clathrin and clathrin bound in cages are in thermal equilibrium if they have equal chemical potentials in both states. Following similar theories for the self-aggregation of amphiphiles and viral capsids (50,51), the rotational and vibrational parts of the free energy are expected to make relatively minor contributions to the free energy change between free and bound clathrin and are therefore ignored. The Helmholtz free energy of N free clathrin triskelia dispersed in a volume V is then given by:

$$A_{\mathrm{f}}(N, V, T) = -k_{\mathrm{B}}T\ln\left(\frac{V^N}{\Lambda_{\mathrm{f}}^{3N}N!}\right) + N\varepsilon_{\mathrm{f}}, \tag{8}$$

with ε_{f} the solvation energy per clathrin. The thermal de Broglie wavelength is defined by

$$\Lambda_{\mathrm{f}} = \frac{h}{\sqrt{2\pi m k_{\mathrm{B}}T}}, \tag{9}$$

where h is Planck's constant and m the mass of a clathrin. The partial derivative,

$$\mu_{\mathrm{f}} = \left(\frac{\partial A_{\mathrm{f}}}{\partial N}\right)_{V,T}, \tag{10}$$

yields the chemical potential of a free clathrin.

The free energy for a dispersion of n cages of p clathrin each is given by

$$A_{\mathrm{b}}(n, V, T) = -k_{\mathrm{B}}T\ln\left(\frac{V^n}{\Lambda_{\mathrm{b}}^{3n}n!}\right) + np\varepsilon_{\mathrm{b}}, \tag{11}$$

where ε_{b} denotes the combined clathrin–clathrin and clathrin–solvent potential energy of a clathrin in a cage, and with the thermal de Broglie wave length of a cage given by $\Lambda_{\mathrm{b}} = \Lambda_{\mathrm{f}}/\sqrt{p}$. The chemical potential of a bound clathrin reads as

$$\mu_{\mathrm{b}} = \frac{1}{p}\left(\frac{\partial A_{\mathrm{b}}}{\partial n}\right)_{V,T}, \tag{12}$$

where the prefactor corrects for the p clathrin molecules per cage. Balancing the two chemical potentials gives

$$c_{\mathrm{f}} = c_{\mathrm{b}}^{1/p}\left(\frac{m}{\Lambda_{\mathrm{f}}^3}\right)^{1-\frac{1}{p}} p^{-\frac{5}{2}p}\exp\left(\frac{\Delta\varepsilon}{k_{\mathrm{B}}T}\right), \tag{13}$$

where $c_{\mathrm{f}} = mN_{\mathrm{f}}/V$ and $c_{\mathrm{b}} = mpn/V$ denote the concentrations (unit: kg/m^3) of free and bound clathrin, respectively, and $\Delta\varepsilon = \varepsilon_b - \varepsilon_f < 0$ is the potential energy change per clathrin upon inclusion in a cage. In combination with the mass conservation law for the total clathrin concentration,

$$c_{\mathrm{tot}} = c_{\mathrm{f}} + c_{\mathrm{b}}, \tag{14}$$

one readily calculates the concentrations of free and bound clathrin as functions of the total clathrin concentration, as illustrated in Figure 8.

The CAC is conveniently defined from the intersection point of the curves in Figure 8 as the concentration of free clathrin at which this concentration equals the

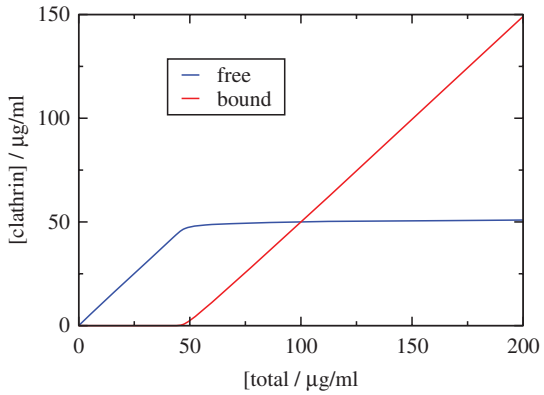

Figure 8: Concentrations of free and bound clathrin, following the derivation of *Appendix 2: Critical Assembly Concentration.* The curves have been calculated assuming a CAC of 50 μg/mL and cages containing $p = 60$ triskelia. The transition to a plateau becomes sharper, and the small slope of the plateau diminishes, with increasing cage size.

concentration of bound clathrin. As the graph shows, the concentration of free clathrin nearly stabilizes at a plateau level close to the CAC for total concentrations exceeding the CAC. By using the experimental plateau value of 50 μg/mL (22) as the CAC value, we obtain from Eq. 13 that the energy released per clathrin upon binding to a cage, i.e. $-\Delta\varepsilon$, is ∼42 $k_B T$ for small cages of 36 triskelia, and nearly 43 $k_B T$ for cages of 100 clathrin molecules, which compares reasonably well with the ∼23 $k_B T$ obtained from the simulations.

A more detailed derivation for capsids shows that intermediate half-completed cages, which were ignored in the current analysis, are thinly populated and hence of little consequence (51,52). We further note that clathrin, unlike many viruses, are capable of assembling in a variety of cage sizes p, and even for a given size can produce a number of distinct structures, i.e. with different distributions of the pentagons relative to the hexagons (53), which has been ignored in the current order-of-magnitude analysis.